

Effect of Prolonged Isothermal Exposure on Elevated-Temperature Time-dependent

Fatigue Crack Propagation in INCONEL alloy 783

Longzhou Ma*, Keh-Minn Chang**, and Sarwan K. Mannan***

* Harry Reid Center for Environmental Studies

University of Nevada, Las Vegas, NV 89154, USA

** Mechanical and Aerospace Engineering Department

West Virginia University, Morgantown, WV 26506, USA

*** Special Metals Corporation, Huntington, WV 25705, USA

Abstract

The effect of isothermal exposure on elevated-temperature time-dependent fatigue crack propagation (FCP) in INCONEL[®] alloy 783 is investigated. Commercially produced alloy 783 was annealed and aged following the standard heat treatment procedure. One set of specimens was then isothermally exposed at 500°C for 3000 hours. Both set of specimens were subjected to FCP tests with various hold time periods and sustained loading crack growth tests at 538°C and 650°C in laboratory air environment. Without hold time, as produced and isothermally exposed materials had comparable fatigue crack growth rates (FCGR) at both test temperatures. With hold times of 100s and 300s, as-produced and isothermally exposed specimens had comparable FCPR at 538°C. Hold time testing of as-produced material at 650°C showed abnormal time-dependent FCP and sustained loading crack growth retardation. However, hold time testing of isothermally exposed material at 650°C showed steady sustained loading crack growth and full time-dependent FCP typically observed in many superalloys. Comparison with alloy 718 data from the literature shows that FCP rates of as-produced alloy 718 and isothermally exposed alloy 783 are comparable at 650°C. A full time-dependent FCP model based on the damage zone concept and thermal activation equation is proposed to characterize the fatigue crack growth behaviors.

® INCONEL is a trademark of Special Metals Corporation.

I. INTRODUCTION

Over the past twenty years, the initial successful development and application of low coefficient of thermal expansion (CTE) iron-nickel based superalloys such as INCOLOY® alloys 903, 907, and 909 have significantly improved the efficiency of aircraft engine by controlling clearance between turbine or compressor blade tips and outer seals and shrouds. Since Cr lowers the Curie temperature and increases CTE, these low CTE superalloys contain only a residual level Cr. Consequently, these alloys are susceptible to stress accelerated grain boundary oxidation (SAGBO) ^[1-4] as well as high rate of general oxidation. Recently developed INCONEL alloy 783 is a result of a development program aimed at improving the resistance to SAGBO while maintaining a low CTE. Alloy 783 is unique since it contains very high aluminum (5.4 wt%) compared to conventional low CTE superalloys such as INCOLOY alloys 903, 907 and 909. Al results in precipitation of NiAl-type β in austenite matrix in addition to Ni₃Al-type γ' . It was previously reported that thermomechanical processing could be used to tailor the morphology and distribution of β phase to improve SAGBO resistance of alloy 783, while providing low thermal expansion and useful mechanical properties up to 600°C ^[1,4]. Also, the high Al content reduces density to 7.81g/cm³, which is 5.0 % lower than alloy 718. Due to its low CTE, high strength, and good oxidation resistance, alloy 783 has been specified by several commercial aircraft gas turbine industries. The alloy is currently specified for aircraft casings, shrouds and seals and has been considered for use in similar industrial turbine components.

Gas turbine components made of superalloys experience thermal exposure of up to 600°C for times to 30,000 hours or more under service conditions. Therefore, the effect of prolonged thermal exposure on properties of superalloys is of great interest to engine designers. Radavich^[5] and Zheng^[6] have pointed out that exposure of alloy 718 at 650°C for 800 hours in air enlarged γ' [Ni₃AlNb] precipitate size, which remarkably improved intergranular cracking resistance.

Mannan and deBarbadillo reported that the prolonged isothermal exposure of alloys 718,783 and 909 decreased high temperature elongation by about 10-20%^[4].

It is well documented that FCP of most superalloys shows time-dependent behavior when a hold at maximum load is introduced or the frequency is decreased. Under time-dependent conditions, the FCP rate is dramatically enhanced and the crack propagation path becomes intergranular. Since FCP shows a cycle-dependent mode in vacuum under hold time fatigue conditions, SAGBO is thought to be responsible for the time-dependent FCP behavior in most superalloys^[7-9]. When the crack tip is subjected to a fatigue cycle with a hold time at maximum load at elevated temperature, oxygen in air is thought to diffuse into materials preferentially along grain boundaries during holding, resulting in a damage zone ahead of crack tip^[9,10]. After holding, the following cyclic loading (unloading and uploading) causes the fast crack advancement within the damage zone. The crack path shows the intergranular mode inside the damage zone. The formation and propagation kinetics of damage zone essentially governs the time-dependent FCP process. The objective of this study is to examine the effect of prolonged isothermal exposure on FCP behavior of alloy 783 at elevated temperature under time-dependent condition, and thereby evaluate the influence of isothermal exposure on SAGBO resistance of alloy 783. Finally, a general model for characterization of FCP behavior of alloy 783 subjected to standard heat treatment and prolonged isothermal exposure is proposed.

II. Materials and experimental procedures

A. Materials and Heat treatments

Hot rolled flats of INCONEL alloy 783 were supplied by Special Metals Corporation, Huntington, WV. Analyzed chemical composition of alloy 783 in weight percentage was Co-28Ni-25Fe-5.3Al-3Nb-3Cr-0.3Ti. The blank samples were cut from as-rolled flats and were subjected to a standard heat treatment as follows: Material was annealed at 1120°C for 1 hour and quenched in water. Then, the annealed material was heat treated 843°C for 4 hours and cooled in

air. This heat treatment precipitated β phase. After β aging, the material was heated to 720°C for 8 hours and cooled in furnace at a rate of 55°C/hr to 620°C, held for 8 hours and then cooled in air. This procedure is called γ' aging, which results in the formation of γ' in the matrix. After the standard heat treatment, one set of specimens was subjected to isothermal exposure at 500°C for 3000 hours. All samples were machined into single edge notched (SEN) fracture specimens with width of 19.05 mm, length of 69.85 mm, thickness of 3.18 mm, and notch depth of 3.81 mm. All specimens were fatigue precracked up to 2.5 mm using a low constant cyclic stress intensity factor ($\Delta K=22.5 \text{ MPa}\sqrt{\text{m}}$) at room temperature. Hot rolled and heat treated microstructures were examined by an optical microscope and scanning electron microscope (SEM). Samples were sectioned and mounted for polishing following standard laboratory procedures. Kalling's reagent containing 6 gm CuCl_2 , 100 ml HCl , 100 ml H_2O , and 100 ml CH_3OH was used to reveal the microstructure. Optical microscopy was done with a Leitz Laborux 12 ME optical microscope equipped with a CCD camera and a PC computer for digital recording. A Hitachi S-750 SEM was used to examine the fracture surface and β precipitates morphology.

B. Fatigue Crack Propagation (FCP) Test

FCP tests were conducted at 538 °C and 650°C. Sinusoidal and trapezoidal cycle variations with different hold time periods at maximum load are schematically illustrated in Fig.1. After reaching the test temperature, a precracked specimen was loaded by a sinusoidal 3s fatigue and crack length was allowed to grow up to a minimum of 2.5 mm so that a steady crack growth rate could be determined. Following the 3s cycle, a hold time fatigue was applied. After the crack length propagated to another 2.5 mm under the hold time cycle condition, a 3s fatigue was imposed again. This procedure allowed the previous testing history to be removed. Then, another hold time fatigue with a longer period was introduced to generate another steady crack growth rate. Constant stress intensity factor (K) was used in all the cases. During FCP test, the maximum

stress intensity factor (K_{max}) and ratio of minimum load to maximum load (R) were kept at 38.5 MPa \sqrt{m} and 0.05 respectively. Crack length was monitored by a D.C potential drop technique linked to a MTS servo-hydraulic system. This system is fully controlled by a computer with a measurement resolution of about 5-10 μm and an error of less than 10%. A quartz heater mounted on MTS provided a uniform temperature across the specimen with a fluctuation of $\pm 5^\circ C$.

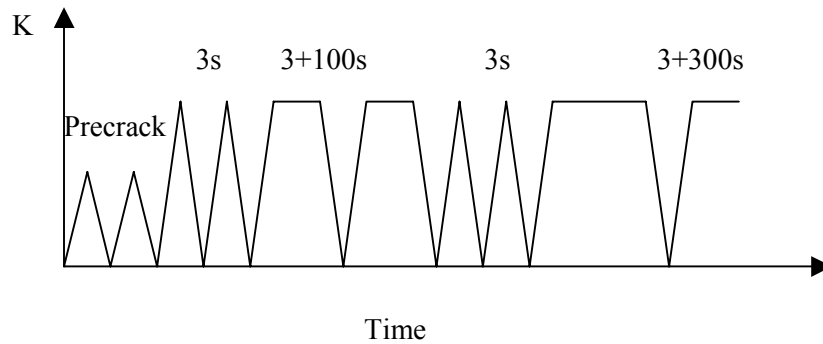


Fig.1. Schematic illustration of FCP test procedure

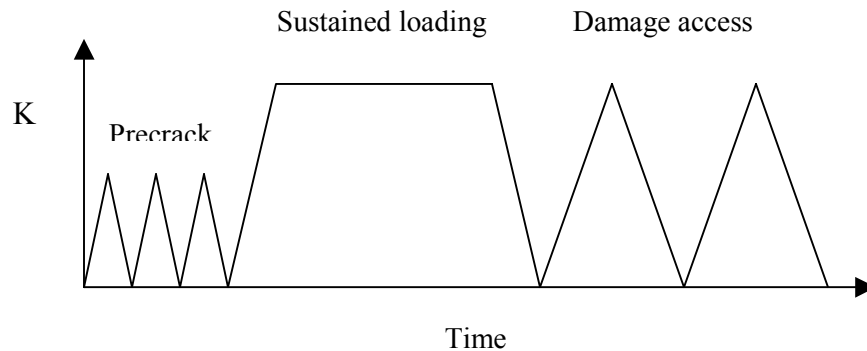


Fig.2. Schematic illustration of damage access test

B. Damage Access Test

Fig.2 shows a damage access test procedure based on damage zone model designed to measure the damage zone size caused by the sustained loading. The specimens were fatigue precracked at

room temperature by a low constant cyclic stress intensity factor ($\Delta K=22.5 \text{ MPa}\sqrt{\text{m}}$) with a frequency of 10 Hz and a load ratio of 0.1. This was followed by high temperature crack growth test at sustained load for a sufficient period to measure steady sustained loading crack growth rate. The stress intensity factor used was ($K_{\text{max}}=38.5 \text{ MPa}\sqrt{\text{m}}$), which is greater than the threshold static crack growth of alloy 783 ^[1,13]. The crack was allowed to grow up to 2.5 mm. After the sustained loading, the specimens were cooled to room temperature and subsequently a normal fatigue with the same value of K_{max} ($K_{\text{max}}=38.5 \text{ MPa}\sqrt{\text{m}}$), and a frequency of 1/6 Hz and a load ratio of 0.1 were introduced. The monitor system was able to record the crack growth cycle-by-cycle for a frequency of 1/6 Hz. Since K_{max} was kept same as the sustained loading crack growth test, the crack grew instantly without incubation induced by the plastic zone. The fatigue crack growth behavior was used to evaluate the damage zone size caused by the previous sustained loading. In this case, the following fatigue crack growth behavior corresponded to a maximum or critical value of damage zone size ^[9,10]. All specimens were broken into two halves after the testing. The measurement of beach marks associated with various testing conditions was made for crack length and K value calibration. In addition to crack growth tests, the tensile properties and hardness were measured at room temperature.

III. Results

A. Microstructure and Tensile Properties

The optical microstructures of isothermally exposed and as-produced samples are shown in Fig.3. Isothermally exposed and as-produced samples show an isotropic microstructure with a similar grain size of ASTM 5-7. SEM photograph shows numerous bar-like β precipitates networks formed on grain boundaries, Fig.4. These precipitates are likely to have formed on β aging mentioned earlier. Since the solvus temperature of β phase is approximately 1175°C and the annealing temperature is 1121°C, globular β particles formed during processing were not completely dissolved during annealing are shown in the matrix and on the grain boundaries. As-

produced and isothermally exposed samples show an identical morphology of β precipitates. Table II shows the effect of isothermal exposure on tensile properties of alloy 783 at room temperature. Prolonged isothermal exposure marginally increased the yield strength and lowered the elongation.

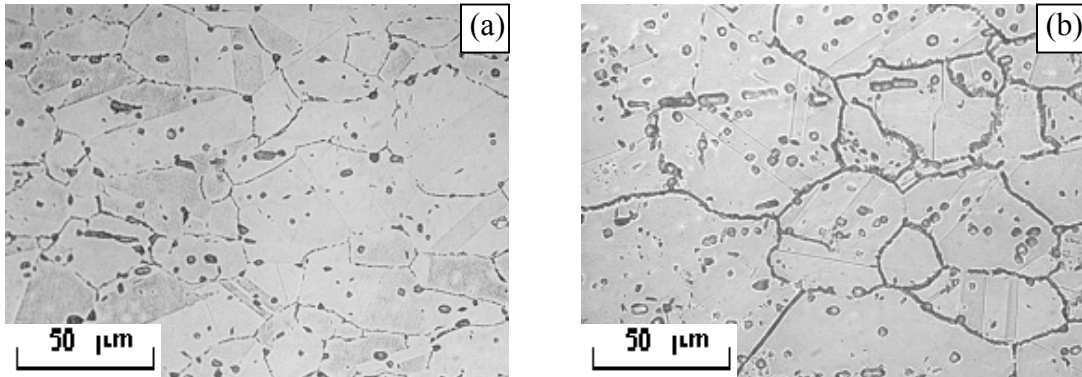


Fig. 3 Optical microstructure of alloy 783

(a). Isothermally exposed; (b). As-produced

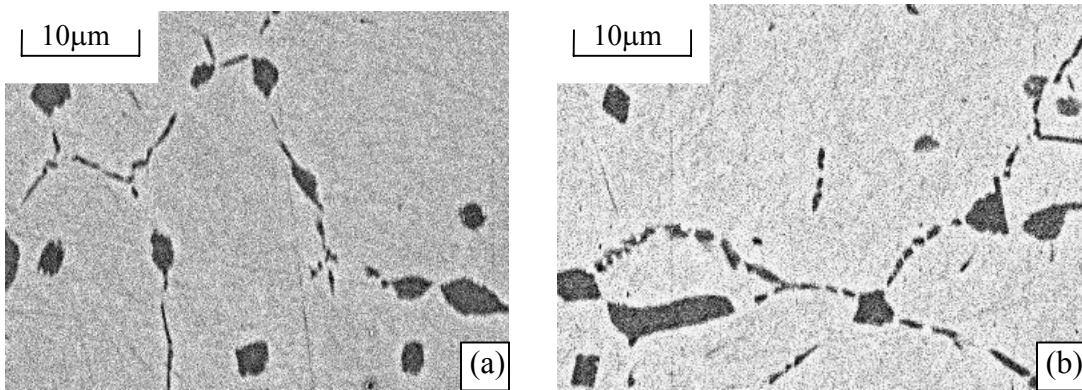


Fig. 4 SEM micrograph of β precipitate

(a). Isothermally exposed; (b). As-produced

Table II. Comparison of alloy 783 Tensile Properties and Hardness at Room Temperature

Treatment	$\sigma_{0.2}$, MPa	σ_b , MPa	δ , %	Hardness, HRC
Isothermally exposed	953	1236	20.2	34
As-produced	852	1225	25.9	31

B. Fatigue Crack Propagation (FCP)

A ΔK controlling FCP curve at 650°C for isothermally exposed specimen is shown in Fig.5. The slope of the linear portion of each curve represents the fatigue crack growth rate, da/dn . As the cyclic stress intensity factor (ΔK) was kept constant, the crack propagated at a constant rate. In Fig. 5, the time-dependent FCP is evident and the steady fatigue crack growth rate increases with the hold time period.

FCP rate as a function of cycle period under various hold time periods at 650°C and 538°C are shown in Fig. 6. Both isothermally exposed and as-produced specimens exhibit the time-dependent FCP behavior, i.e. FCP rate (da/dn) is a function of the period of cycle. Theoretically, a linear relationship between FCP rate (da/dn) and period (t) will be established when the hold time reaches above a critical value, i.e. FCP is fully time-dependent ^[10]. Temperature usually plays a significant role in time-dependent FCP. The increase of temperature can promote the occurrence of time-dependent FCP at a shorter period and cause a higher FCP rate. Fig. 7 compares the effect of isothermal exposure on FCP rate at different temperatures. At condition of 3s cyclic load, the FCP rates of isothermally exposed and as-produced specimens are comparable at both temperatures. With hold times of 100s and 300s, as-produced and isothermally exposed specimens showed comparable FCGR at 538°C. However, under hold times of 100s and 300s, prolonged isothermal exposure increased the time-dependent FCP rate at 650°C.

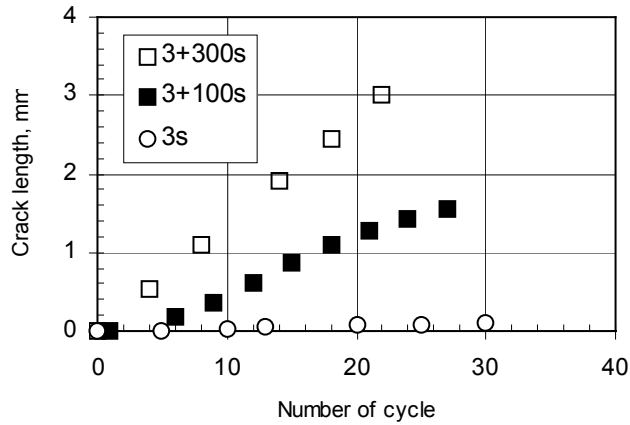
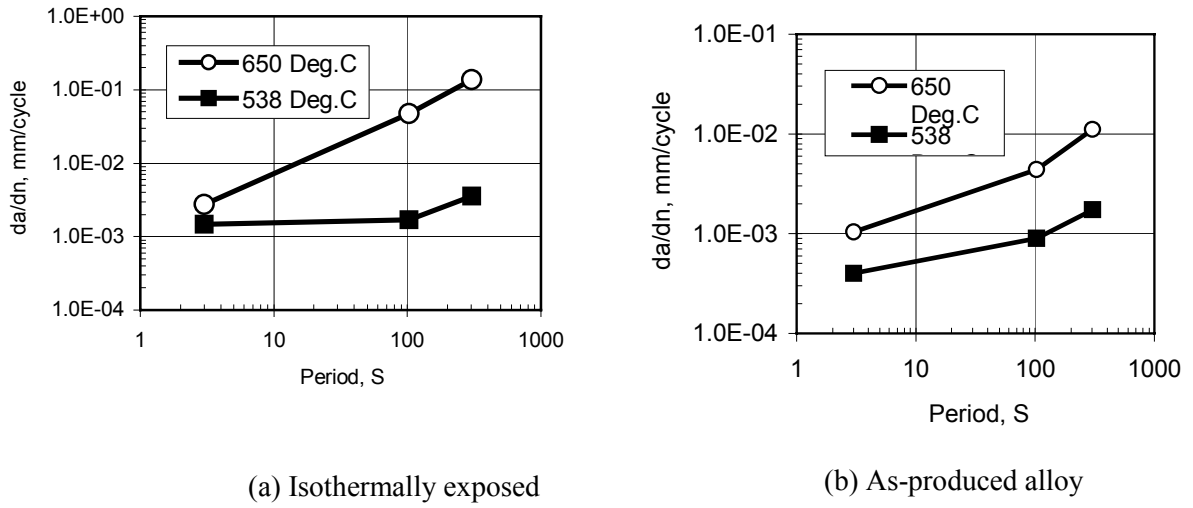


Fig. 5. FCP curves of isothermally exposed material at $K_{max}=38.5 \text{ MPa}\sqrt{\text{m}}$ and 650°C



(a) Isothermally exposed (b) As-produced alloy

Fig. 6. Fatigue crack growth rate as a function of period, S

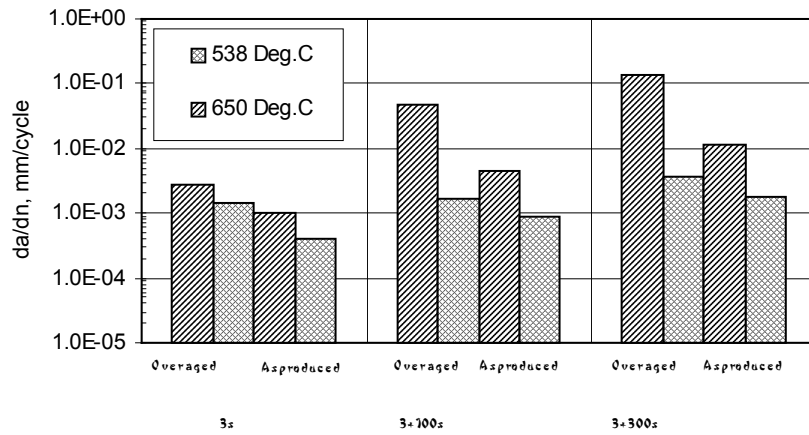
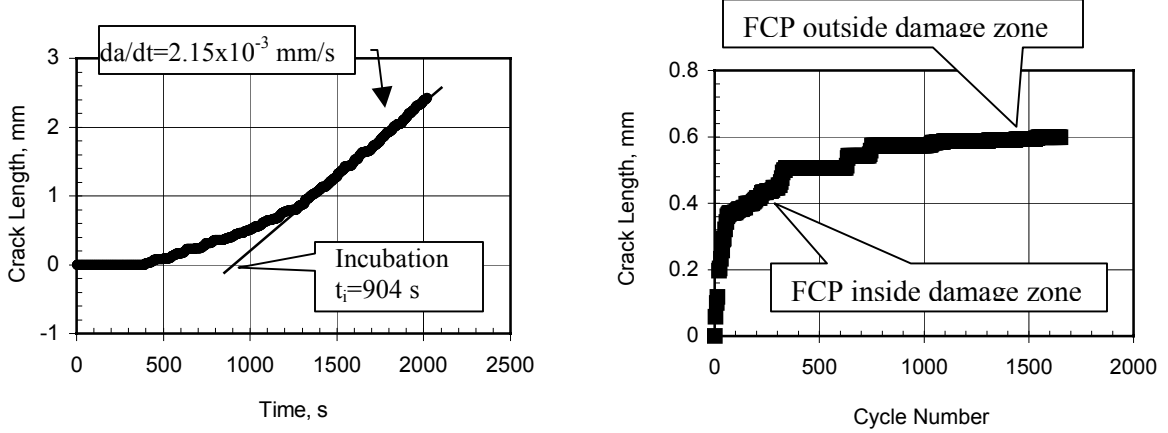


Fig. 7. Comparison of fatigue crack growth rate of isothermally exposed and as-produced alloy 783 at $K_{max}=38.5 \text{ MPa}\sqrt{\text{m}}$. Over aged stands for isothermally exposed.

C. Sustained loading crack growth and damage access

The sustained loading crack growth rate (da/dt) can be viewed as an important reference for time-dependent FCP rate (da/dn). Mathematically, at full time-dependent stage, the sustained loading crack growth rate (da/dt) can be used to relate with the time-dependent FCP rate (da/dn)^[14, 15]. Actually, the sustained load can be considered as a specific type of hold time fatigue cycle with an extremely long hold time period. Therefore, insight into the sustained loading crack growth process can assist understanding of the time-dependent FCP behavior. Following the testing procedure illustrated in Fig. 2, isothermally exposed specimens were damage access tested as shown in Fig. 8. In this test, the crack length remains unchanged for about 500 seconds after receiving a static K_{max} , Fig 8 (a). It takes about 900 seconds to reach the steady crack growth. As the sustained load K_{max} was kept constant, the crack propagated linearly. The slope of the linear portion of crack growth curve represents the steady crack growth rate, da/dt . The intersection between the steady crack growth line and the horizontal line represents the incubation time (t_i), wherein the crack starts to grow stably. Fig. 8(b) shows FCP behavior at room temperature following the sustained loading crack growth test. Since K_{max} was kept the same as the sustained loading test, the fatigue crack propagated immediately without any fatigue incubation caused by plastic zone. The zero cycle refers to the end of sustained loading crack growth test. The crack length represents the crack increment at the condition of 6s fatigue. As displayed in Fig. 8 (b), FCP exhibits a remarkably different behavior compared to the linear steady FCP shown in Fig. 5. In the beginning of the test, the fatigue crack grew at a very fast rate, and then the growth rate gradually slowed down with the increase of crack length. Eventually, the crack growth rate returned to a stable value and the crack propagated again in a linear relationship between the crack length and the number of cycle. The distance from the end of sustained loading to the beginning of a normal crack growth is defined as the damage zone, inside which the fatigue crack growth is accelerated.



(a). Sustained loading crack growth at 650 °C (b). Damage zone identification at room temperature

Fig. 8: Damage access result of isothermally exposed alloy 783 at $K_{max}=38.5$

Fig. 9 represents the sustained loading crack growth rate (da/dt) and the inverse of incubation period ($1/t_i$) as a function of temperature. The data of alloy 718 at K_{max} equal to $40.0 \text{ MPa}\sqrt{\text{m}}$ is taken as a reference [16]. As expected, a high value of da/dt and low value of t_i are observed at high temperature. Therefore, a thermal activation Arrhenius equation can be employed to correlate the measured sustained loading crack growth rate (da/dt) and incubation period ($1/t_i$) as follows:

Sustained loading crack growth rate, da/dt :

$$\frac{da}{dt} = C \cdot \exp\left(\frac{-Q}{RT}\right) \quad (1)$$

Incubation period, $1/t_i$:

$$\frac{1}{t_i} = A \cdot \exp\left(\frac{-Q}{RT}\right) \quad (2)$$

where, A and C are constants, T is absolute temperature, R is gas constant, and Q is thermal activation energy. Fig.10 represents the variation of the critical damage zone size developed during sustained loading crack growth with temperature. Actually, a large amount of

experimental data in alloy 718 has verified that the damage zone size (x) had a linear relationship with holding period (t) as shown in equation (3) [9,10].

$$x = B \cdot t \cdot \exp\left(\frac{-Q}{RT}\right) \quad (3)$$

where B is a constant. In Figs.9 and 10, although the data points are relatively closely spaced, the fact that those lines are almost parallel to each other suggests that the sustained loading crack growth, incubation process, and formation of the critical damage zone are rate-controlled thermal activated processes. For isothermally exposed alloy 783, the slope of lines in Figs.9 and 10 give an average Q value of about 242 KJ/mole. The value of Q has been reported to be 255 KJ/mole for the formation of damage zone of alloy 718 superalloys [10,11].

Interestingly, the as-produced specimen did not show significantly detectable crack growth under sustained loading condition at 650°C as seen in Fig. 11. The crack length was almost unchanged for over 100 hrs, although there was a very slight crack extension after 3000 hrs. This phenomenon, defined as crack growth retardation [12, 13], took place at 538°C under sustained loading condition as well.

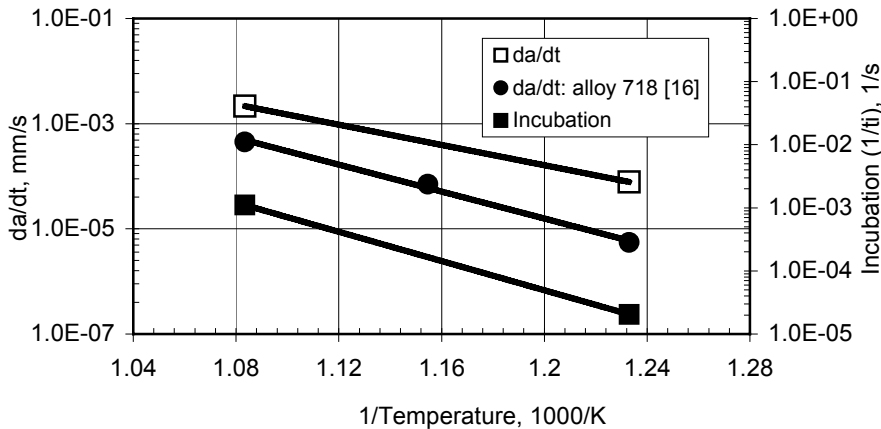


Fig. 9 da/dt of isothermally exposed alloy 783 vs.1/T

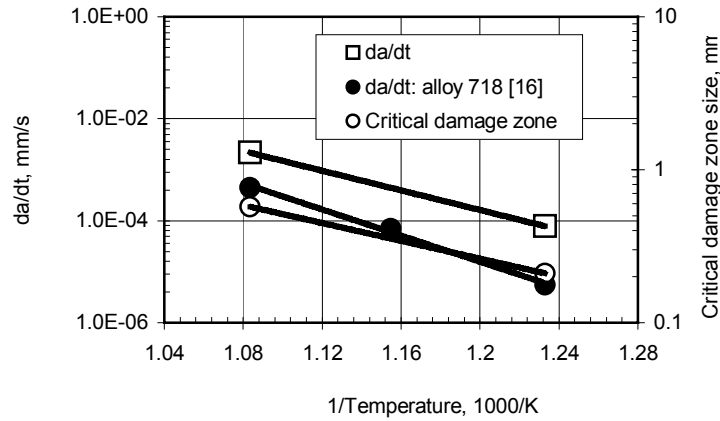
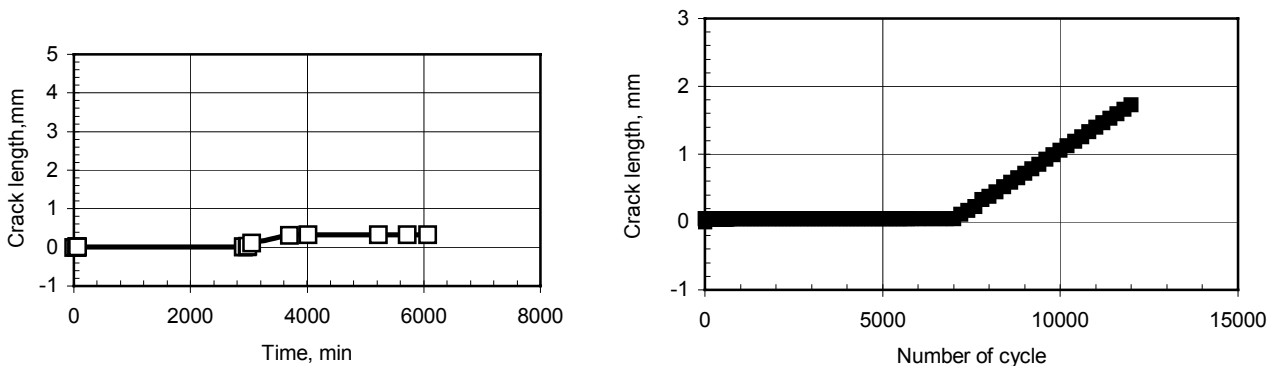


Fig. 10 da/dt of isothermally exposed alloy 783 vs. $1/T$ for damage zone size

Following the sustained loading as shown in Fig 11 (a), the result of damage access test as seen in Fig. 11 (b) displays the normal stable fatigue crack growth with an incubation of about 7000 cycles instead of the instantly accelerated crack growth caused by the presence of damage zone as shown in Fig.8 (b). The fact that FCP was delayed and there was a fatigue incubation of 7000 cycles in damage access test suggested that there existed a crack retardation zone ahead of crack tip developed during the sustained loading rather than a damage zone. The fatigue crack did not propagate until the crack retardation zone was overcome by an accumulation of the mechanical damage with 7000 fatigue cycles



(a) Sustained loading crack growth retardation at 650°C (b) Delayed FCP following (a) at room temperature

Fig. 11 Damage access result of as-produced alloy 783 at $K_{max}=38.5 \text{ MPa}\sqrt{\text{m}}$

D. Full time-dependent FCP Identification

As illustrated above, both as-produced and isothermally exposed samples demonstrate the time-dependent FCP behavior. If an alloy shows the time-dependent FCP component under hold time condition, further increase in hold time period will result in a faster FCP rate. Eventually, FCP becomes fully time-dependent and the FCP rate, da/dn , shows a linear relationship with the hold time length, i.e. da/dn could be mathematically associated with sustained crack growth rate (da/dt). However, unlike isothermally exposed alloy 783, as-produced alloy displays the sustained loading crack growth retardation and a retardation zone instead of the steady sustained loading crack growth and a damage zone. This observation is completely different from the conventional concept of time-dependent FCP in most superalloys. In order to confirm the validation of crack growth retardation at the condition of sustained loading, FCP tests of as-produced samples were conducted with prolonged hold time period ranging from 100 to 1000 s at 650°C according to the FCP testing procedure as illustrated in Fig.1. The gradual increase of hold time length allows the fatigue cycle to approach the sustained loading status, which can be considered as a particular cycle with an extreme hold time length, i.e. $t \rightarrow \infty$. Fig. 12 shows the FCP testing results of as-produced alloy 783 at 650°C and $K_{max}=38.5 \text{ MPa}\sqrt{\text{m}}$. When hold time length is less than 1000s, FCP is time-dependence with a steady growth rate. However, no steady crack growth was detected for about 160 cycles (about 45 hours) at 3+1000s, although there was a little crack extension initially during the 50 cycles.

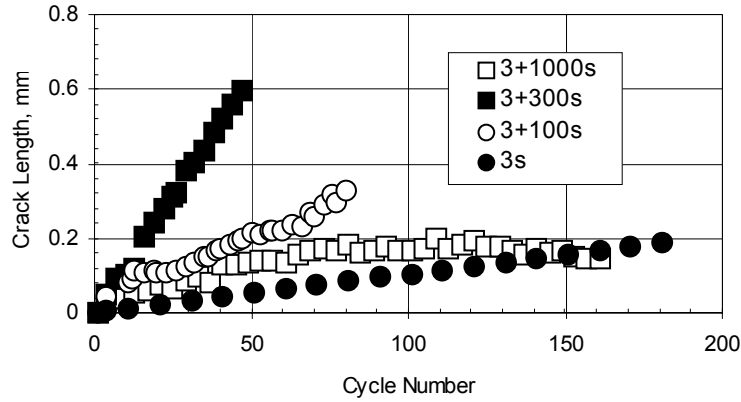


Fig. 12 FCP curves of as- produced alloy 783 at $K_{max}=38.5 \text{ MPa}\sqrt{\text{m}}$, $R=0.05$ and 650°C

To identify the full time-dependent FCP behavior, the FCP rate, da/dn , was rewritten as

$\frac{da}{dn} = t \times \frac{da}{dt}$, wherein t is period of fatigue. Fig. 13 plots the static crack growth rate (da/dt),

transformed by $\frac{da}{dt} = \frac{1}{t} \times \frac{da}{dn}$ using data in Fig 7, Fig. 9, Fig.11 and Fig. 12, as a function of cycle

period. In order to plot all experimental data in one graph, t_∞ represents the period of sustained loading, and a specific value of da/dt , $1 \times 10^{-8} \text{ mm/s}$, stands for the crack growth retardation in

Fig.13. Considering the experimental scatter, the constant static crack growth rates (da/dt) of isothermally exposed alloy 783 suggests that FCP falls in the full time-dependent domain,

wherein the sustained loading crack growth rate (da/dt) can be used to correlate with the FCP rate (da/dn). Furthermore, Fig. 13 shows that the time-dependent FCP of isothermally exposed sample even starts at 3s fatigue. In contrast, as-produced alloy displays an abnormal FCP

behavior that consists of three portions, the cycle-dependent portion, time-dependent portion, and crack growth retardation portion. When hold time is shorter than 100s, fatigue crack grows at a cycle-dependent mode. Increasing hold time period allows FCP to show the time-dependent

mode. Further increasing the holding period to 1000s results in the crack growth retardation. Fig. 13 shows the full time-dependent FCP behavior of isothermally exposed alloy 783, but also confirms the observation that further increasing the hold time length will cause the crack growth

retardation in as-produced alloy. The abnormal FCP behavior of as-produced alloy also occurs at 538°C as shown in Fig. 14. Lower temperature allows the time-dependent FCP to occur at a longer period, 100s. FCP of isothermally exposed alloy will approach the full time-dependent status when the period of fatigue reaches a critical value such as 100s, but as-produced alloy only demonstrates an abnormal FCP with the increase of period.

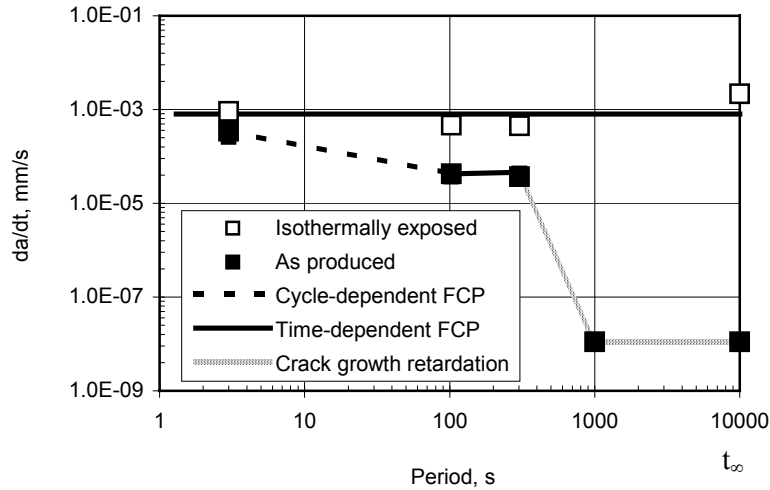


Fig. 13 Time-dependent FCP at $K_{\max}=38.5 \text{ MPa}\sqrt{\text{m}}$ and 650°C

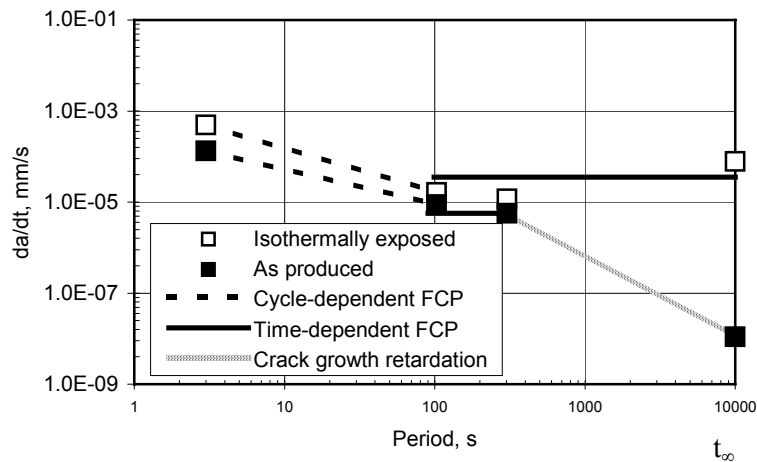


Fig. 14 Time-dependent FCP at $K_{\max}=38.5 \text{ MPa}\sqrt{\text{m}}$ and 538°C

VI. Discussion

A. Stress Relaxation Examination

One of the important findings in this study is that as-produced alloy 783 displays an abnormal time-dependent FCP and crack growth retardation behavior when the hold time period is prolonged. It has been reported that the crack blunting, which is usually caused by creep deformation ahead of crack tip or heavy corrosion products on the fracture surface, could contribute to the decreased crack growth rate or crack growth retardation in superalloys [12, 17]. Floreen found that the extensive sulfur-containing corrosion products on the crack surface in INCOLOY alloy 800 could cause the crack tip to blunt and thereby retard the sustained loading crack growth [17]. Severe creep deformation in superalloys relaxes the stress field at the crack tip which, decelerates and stops the crack growth [12]. Since isothermal exposure increased yield strength as shown in Table II, the crack growth retardation in as-produced specimens is perhaps associated with the creeping effect. To determine if creep deformation contributes to the crack growth retardation, the tensile stress relaxation behaviors of isothermal exposed and as-produced alloy 783 were examined at 650°C following the testing procedure as illustrated in ASTM E328-86-1991. To measure the tensile stress relaxation, a tensile specimen was loaded in tension with a strain rate of 0.02 mm/s at 650°C. Once the tensile strain reached a value of 4.5%, the crosshead displacement of the MTS was stopped. The position of the crosshead was maintained with a feedback loop, while the load was allowed to drop. The data acquisition system monitored the variation of time and loads, and then stored the data from the testing. After testing, the measured data was processed according to the transformation relationship between stress vs. time and strain rate vs. stress [18]. Fig. 15 shows the analyzed results where the strain rate is plotted as a function of stress. Overlapping of two stress relaxation curves implies that the isothermally exposed and as-produced specimens have identical creep resistance at 650°C. Therefore, it can be inferred that

the different crack growth behaviors of as-produced and isothermally exposed materials under the time-dependent and sustained loading conditions can not be ascribed to creep deformation.

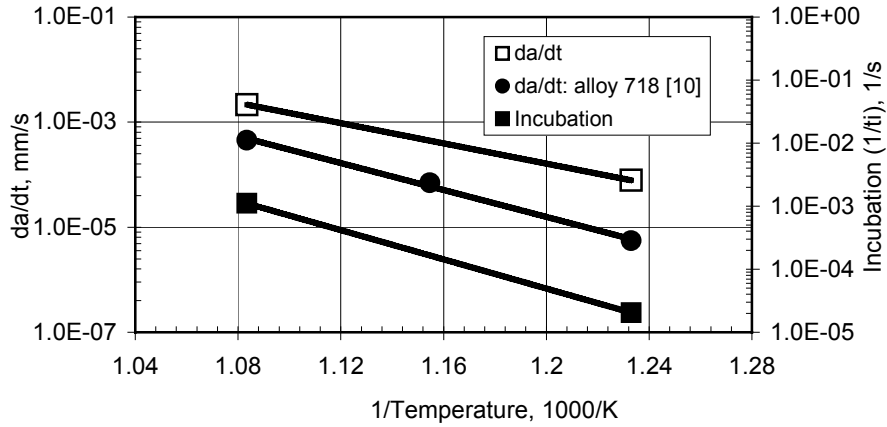


Fig. 15 Tensile stress relaxation at 650°C

B. Fracture surface characterization

Fig. 16 shows the fracture surface of isothermally exposed alloy 783 under different loading conditions. As seen in Fig. 16 (a), there is a clear border between the fracture surface of pre-crack and 3s fatigue. At pre-crack region, the fracture surface displays the conventional fatigue striation. However, when crack propagated at condition of 3s fatigue, the crack path was predominantly intergranular and lots of facets appeared. As the hold time period was imposed, e.g. at 3+100s and 3+300s, the crack paths were fully intergranular and the grain boundaries were faceted. The whole surface was relatively rough and covered by a layer of oxide film, indicating that lots of oxidation occurred during crack growth. Compared to 3+100s, the roughness of fracture surface at 3+300s seemed to be decrease and a few of globular β particles and the same size holes appeared. It suggests that the thickness of oxide film decreased revealing globular β particles and holes. Under sustained loading condition, the typical intergranular fracture was evident, and the roughness of surface and the thickness of oxide film decreased to the minimum, suggesting that cracking behavior was predominant relative to oxidation behavior. Numerous protruding β particles and holes were observed, implying that β particles were separated from

matrix during crack propagation. The clean grain boundary facets suggested that there was only a little cohesion between grain boundaries during fracture.

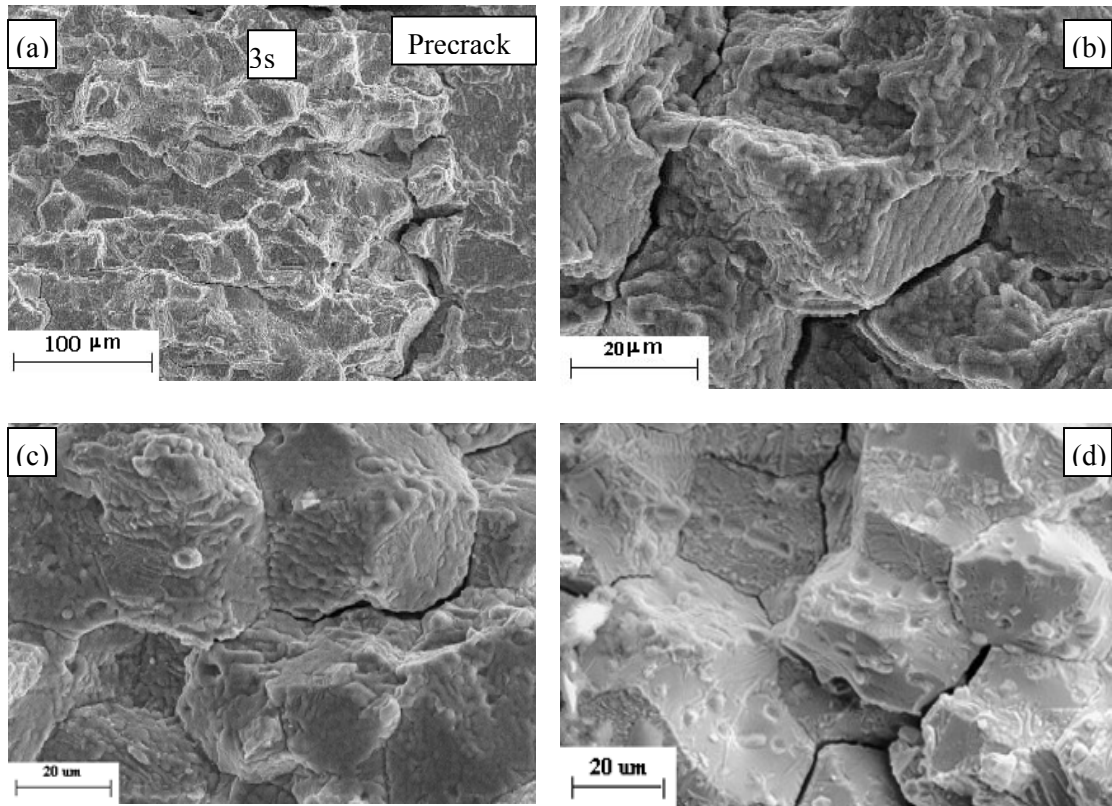


Fig.16. SEM fracture surface micrograph of isothermally exposed alloy at 650°C

(a): 3s: (b): 3+100s: (c): 3+300s: (d): Sustained loading

Fig. 17 shows the fracture features of as-produced alloy 783 subjected to hold time fatigue at 538°C and 650°C. The crack path under 3+100s and 3+300s hold time conditions was intergranular, and the fracture surface at condition of 3s fatigue is predominantly transgranular with a little of intergranular fraction. Many preoxidized global β particles are visible. The fracture surface was rough and covered by lots of oxide products, which were identified as Al-containing oxides by EDX analysis. These Al-containing oxides are believed to be from oxidation asperities of NiAl-type β precipitates. The SEM observation of cross section of a specimen at 3+300s and

538°C showed that the crack propagated by means of the repetitive rupture of the inter- and intragranular β particles.

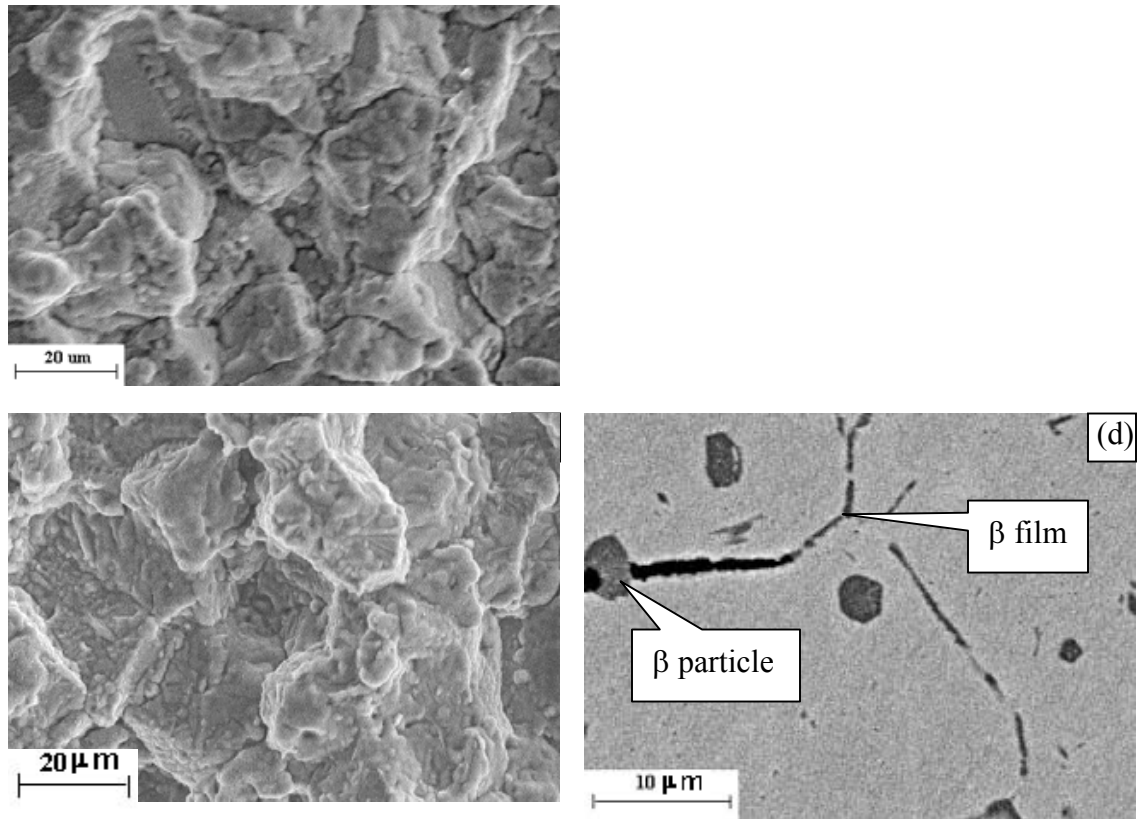


Fig. 17. SEM fracture surface micrograph of as-produced alloy

(a): At 3+100s and 650°C ; (b): At 650°C; (c) High magnification of (b); (d): At 3+300s and 538 °C

When the hold period was increased to 1000s, only a slight crack extension occurred, and then the moving fatigue crack slowed down and eventually stopped the propagation. As seen Fig.18 (a), SEM observation of fracture surface showed the crack extension region was remarkably protruded compared to the flat precrack and 3s fatigue cracking region. High magnification of Fig. 18 (a) exhibited that the protruded region was covered by a large amount of dense oxides. The thickness of oxide film seems to be increased relative to that at both 3+100s and 3+300s as shown in Fig.16. When the hold period was prolonged to a sufficient length, the hold time fatigue approached sustained loading status. As indicated in Fig. 11, crack growth retardation

occurred accompanying with a little crack extension and the “blunt zone” or “retardation zone” instead of the damage zone. The optical microscope observation for the cross section of a specimen subjected to sustained loading crack growth retardation showed that crack propagation was blocked by the inter- and intragranular β particles ahead of crack tip as seen in Fig. 19(a). The specimen was broken into two halves, and fracture surface was examined by SEM. The fracture surface was covered with heavy oxides and the β particles were invisible due to increase of the oxide film thickness, Fig.19 (b).

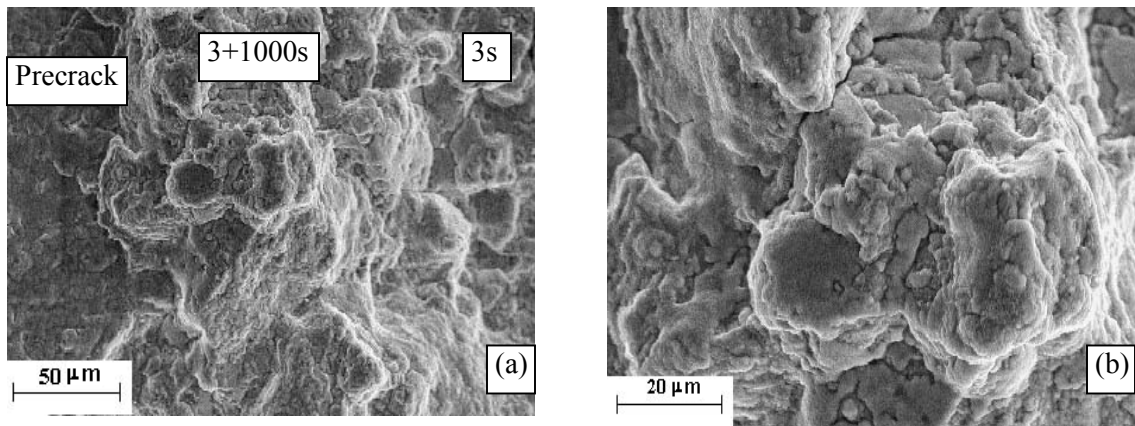


Fig. 18. SEM micrograph of as produced alloy at 650 °C

(a). Crack extension region at 3+1000s

(b). High magnification of (a) at 3+1000s

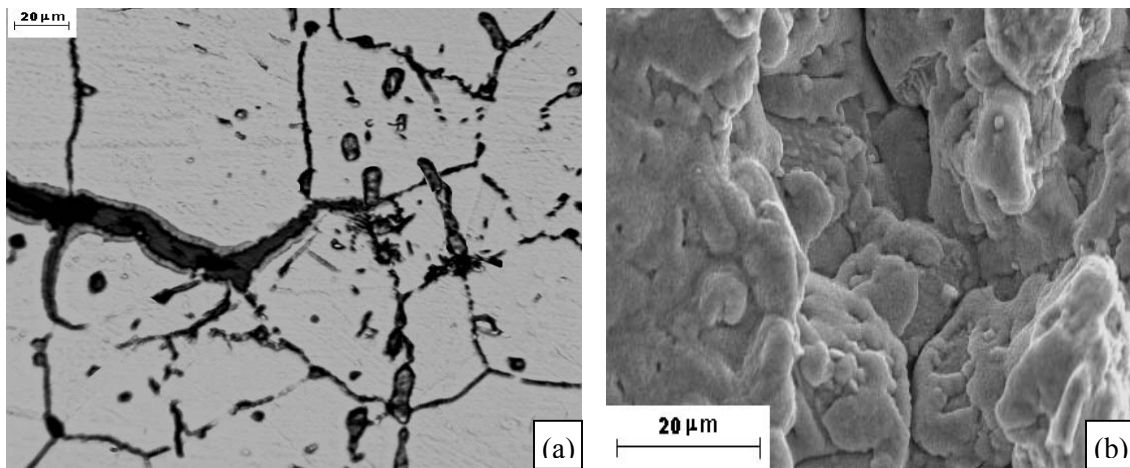


Fig. 19. Sustained loading crack growth retardation of as produced alloy at 650 °C

(a). Optical micrograph of crack path (b) SEM fracture surface micrograph of (a)

C. Proposed cracking mechanism

It is generally agreed that the enhanced time-dependent FCP rate of superalloys caused by hold time is associated with SAGBO, which introduces intergranular fracture. As illustrated in the damage zone model, when a specimen is subjected to a hold time fatigue, oxygen in air is able to penetrate along grain boundary during holding. As a result, a damage zone ahead of the crack tip is formed. After holding, the following cyclic loading (unloading and reloading) permits the crack to advance at a fast rate within the damage zone^[9,10]. The crack advancement rate is related with the degree of damage and damage zone size, which are a function of applied loading, temperature, and hold time. Therefore, a high temperature and long hold time period usually result in a high time-dependent FCP rate. In this study, the existence of a damage zone is evident as shown in Fig. 8 (b). Under time-dependent condition, intergranular fracture mode is responsible for the increased crack growth rate.

As illustrated above, although the grain size and morphology of β precipitates are identical in isothermally exposed and as-produced samples, the crack propagation, especially time-dependent FCP behavior, is different. Isothermally exposed alloy 783 demonstrates a full time-dependent FCP, but as-produced alloy displays an abnormal time-dependent FCP, i.e. the crack growth is retarded at prolonged holding period. Beta precipitates are primarily responsible for abnormal time-dependent FCP in alloy 783^[19-21]. Precipitation of Ni_3Al -type γ' precipitates within β particles on prolonged isothermal exposure^[4] may have been responsible for difference in as-produced and isothermally exposed material. Fig. 20 shows transmission electron microphotographs of Beta particles in as-produced and isothermally exposed alloy 783 from Mannan and deBarbadillo's work^[4].

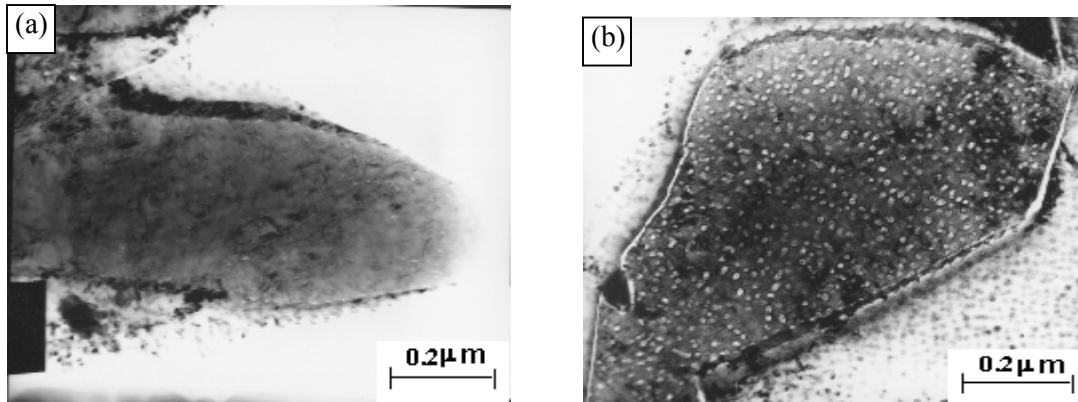


Fig. 20. Transmission electron photograph of β precipitates in alloy 783 from reference #4.

(a) As produced alloy 783 (b) 593°C/1000h exposed

SEM/EDX analysis showed that NiAl-type β precipitates in alloy 783 contained approximately 30% Ni, 24%Co, 15% Fe, and 31% Al by atom percentage^[4]. Since Co and Fe would occupy Ni lattice site, (NiFeCo) Al-type β phase could be Al-rich. Studies have shown that the coating of Al-enriched β phase, during oxidation, can manifest itself as a protective alumina scale (Al_2O_3) to prevent further oxidation at elevated temperature (597-897°C)^[22-24]. Young found that the oxidation process of β phase consists of two stages^[22, 23]. At the first stage of oxidation, the oxide products of NiAl- β intermetallics mainly consist of the porous Ni-containing oxides such as NiAl_2O , NiO and their spinels. These porous oxides, which cannot act as an oxygen diffusion barrier, allow the continuous oxidation reaction to occur in the alloy substrate. At the second stage, the oxygen diffusion toward the fresh material will be prevented due to the establishment of the dense protective alumina scale (Al_2O_3) with the increase of oxidation time. When the construction of the protective alumina layer is fully completed, no further fresh material will be oxidized and the alumina scale is likely to grow by an outward mechanism. The oxygen potential gradient between the scale and gas interface, which is the driving force of the alumina scale growth, will cause both Al and other reactive elements such as Fe, Ni and Cr to diffuse toward the region with high oxygen gradient at the interface. As a result, the scale will keep growing by

outward diffusion of the oxidation-active elements. Usually, the β phase-formed oxide scales consist of, from top to substrate, a layer of thin film containing NiO, and a layer of the oxidized asperities including Al_2O_3 and NiAl_2O . The Al_2O_3 -containing scale has a strong absorption effect to the oxygen penetration and may dilute the oxygen concentration. Pint pointed out that the oxygen-partial-pressure, P_{O_2} , could be reduced from 1 atm to 10^{-29} atm when oxygen diffused to the substrate of NiAl- β intermetallic through the Al_2O_3 dominant alumina scale [25]. For as-produced alloy 783, when the hold time length was not long enough (e.g. $t < 1000\text{s}$), oxygen could preferentially penetrate along grain boundary ahead of crack tip and interact with the intergranular β precipitate film. The oxidation products may predominantly contain the non-protective porous oxides such as NiO, NiAl_2O and their spinels. These oxides could make the local material ahead of crack tip brittle, so a damage zone was formed. After holding, the following unloading and reloading cycle caused the crack to advance forward within the damage zone at an accelerated rate. Therefore, FCP displays the time-dependent behavior, and crack propagates by the repetitive rupture of intergranular β film, which has been already oxidized accompanying with lots of oxides on the fracture surface as seen in Fig. 17. The driving force to break the β film and its oxidized spinels is the cyclic loading, ΔK . Prolonging the holding period (such as 1000s or sustained loading status), the sufficient oxidation time can invoke the protective effect of β phase and form the dense protective alumina layer, Al_2O_3 , against further oxidation. The thickness of the Al_2O_3 -dominant scale increases with hold time by the outward growth mechanism, and eventually crack tip could be filled with these oxidation asperities. Under hold time fatigue condition, the heavy oxides on fracture surface may result in the crack closure, which can lower the driving force (ΔK), and finally retard the fatigue crack growth.

The hypothesis that the crack growth retardation at 3+1000s fatigue is caused by oxide-induced crack closure can be proved by analysis of the data of D.C. potential variation corresponding to the crack growth. In this study, the state-of-the-art monitor system was able to record the load and

potential variation with 500 data points in every single cycle with the acceptable electron noise. Fig. 21 (a) gives an example of the load and potential change as a function of time within a 3s cycle. Three important values of the potential, which respectively correspond to the starting of reloading, maximum loading and ending of unloading, can be recorded in a cycle. Irving and Shih suggested that the change in potential within a cycle could reflect the electrical contact between the fracture surfaces, and thus provide a direct indication of crack closure ^[26,27]. Irving found that any potential drop during a cycle would be due to contact between previously separated crack faces, i.e. crack closure ^[26]. Fig.21 (b) plots the potential drop percentage, Ψ , at minimum unloading relative to the potential at minimum uploading within a cycle as a function of cycle number under various fatigue conditions. When the steady crack growth is observed for example at 3s and 3+100s fatigue, Ψ is too small (around 1.0%) and fluctuated too much to detect any overall trend during tests, suggesting that the crack face may return to the previous location during unloading. However under 3+1000s condition, Ψ significantly increases with the number of cycles eventually reaching 8.0%. The increasing Ψ means that the potential at beginning of reloading is greater than that at ending of unloading, i.e. crack cannot fully close during unloading and premature contact between mating crack planes must occur. Therefore, the crack closure should take place during crack growth under the 3+1000s hold time fatigue condition. Studies have shown that the crack closure could decrease the effective driving force, reduce the crack growth rate, and eventually retardate the crack growth ^[28]. The SEM micrograph of fracture surface at condition of 3+1000s as seen in Fig. 18 exhibits numerous oxide products, which may contribute to the crack closure, are remarkably convex compared to the flat surface at precrack or 3s fatigue.

At sustained loading status, the prolonged exposure period may also cause crack tip to be blunted by forming the oxidation-resistant alumina, Al_2O_3 . The numerous Al-oxide debris can block oxygen penetration and introduce the fracture surface contact ahead of crack tip, and

eventually result in the crack growth retardation. The pileup of intergranular Al_2O_3 -dominant oxides and the grain boundary plate-like β phases are shown in Fig. 19. The fact that the crack tip was blunted extensively during sustained loading could be confirmed by the formation of a “blunt zone” or “retardation zone”, wherein the fatigue crack growth had a incubation of 7000 cycles as shown in Fig. 11 (b). In summary, it is the oxidation characteristics of β phase that essentially contributes to the abnormal time-dependent FCP behavior of as-produced alloy 783.

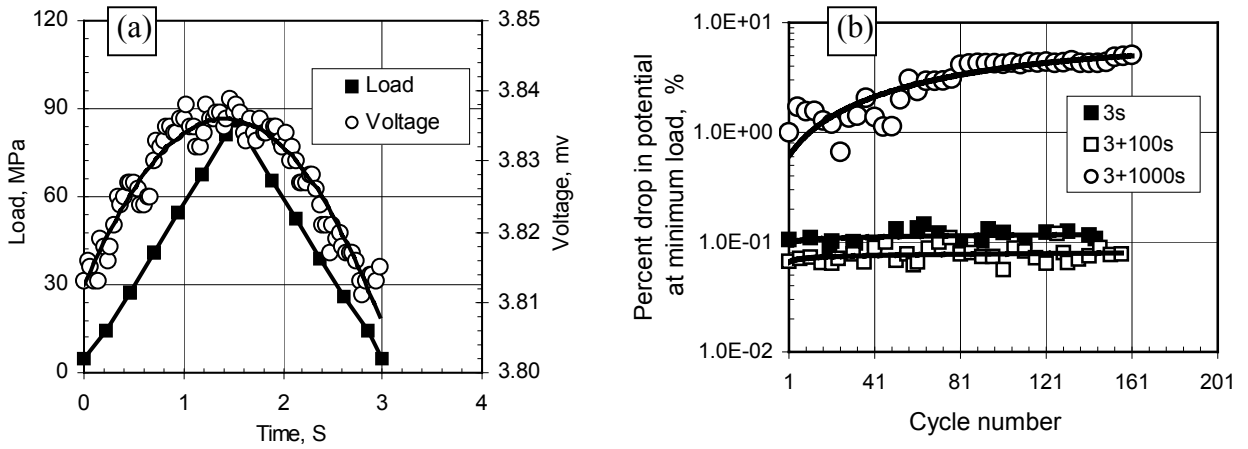


Fig.21. Voltage change during fatigue crack growth test at $K_{\max}=38.5\text{MPa}\sqrt{\text{m}}$, $R=0.05$ and 650°C

(a): Voltage and load change within a fatigue cycle with a period of 3s;

(b): Potential drop at minimum load, Ψ , as a function of cycle number

D. Modeling characterization of time-dependent FCP

On the basis of discussion above, SAGBO induced sustained loading crack growth and time-dependent FCP actually are rate-controlled thermal activation processes associated with the formation and propagation of damage zone ahead of crack tip. Fig. 22 schematically describes this procedure. When a precracked specimen is subjected to a sustained load with a constant stress intensity factor (K_{\max}), the crack cannot grow instantly. Presumably, oxygen in air can preferentially penetrate along the grain boundary and form a damage zone, inside which material

is embrittled and is different from the bulk material due to oxygen deposition. As time passes, the damage zone size and damage degree increases. When the damage zone size reaches a critical value, the crack initiates and starts to grow by cracking the damage zone. Meanwhile, the damage zone continues to grow at the front of crack tip. The steady sustained loading crack growth indicates that the crack propagates at a speed equivalent to the formation of the damage zone, i.e. the consumption and formation of a damage zone reach a balance. When a hold time fatigue is imposed, the crack may or may not grow depending on the incubation during holding time. Nevertheless, a damage zone is developed during holding. After holding, the following unloading and reloading portion of a cycle provides the driving force (ΔK) to fracture the damage zone at an enhanced rate. The cracking rate is a function of applied load, temperature and holding duration. Thus, a higher crack rate will be measured when temperature and holding period increase. Based on the damage zone controlled time-dependent FCP mechanism, a full time-dependent FCP model is proposed by means of a phenomenological approach to characterize the FCP behaviors of the alloys.

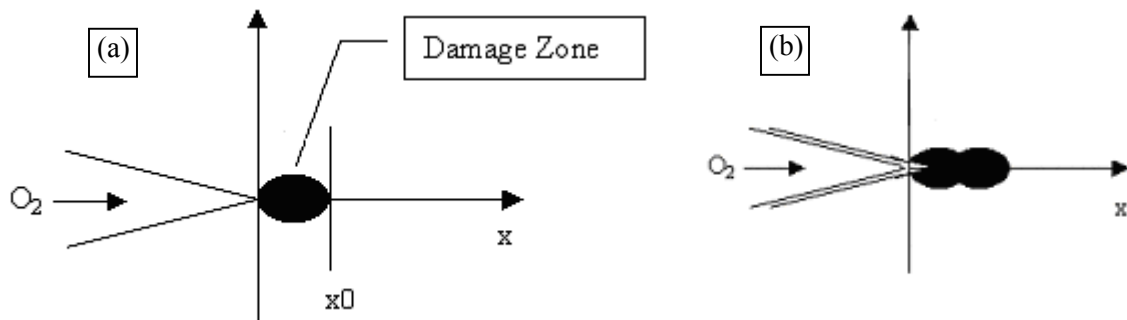


Fig 22. Schematic illustration of the sustained loading crack growth governed by damage zone
 (a). Formation of a critical damage zone during incubation.
 (b). Crack growth by consecutive formation and propagation of a damage zone

According to equation (3), the damage zone size (x) can be expressed as

$$x = B \cdot t \cdot \exp\left(\frac{-Q}{RT}\right)$$

It has been proved experimentally that the sustained loading crack growth rate (da/dt) is equal to the damage zone propagation rate (dx/dt) [9,10]:

$$\begin{aligned} \frac{da}{dt} &= \frac{dx}{dt} \\ \therefore \frac{da}{dt} &= B \cdot \exp\left(\frac{-Q}{RT}\right) \end{aligned} \quad (4)$$

Under the full time-dependent FCP condition, Fig.13 and 14 suggest that the fatigue crack growth rate (da/dn) can be rewritten as:

$$\begin{aligned} \frac{da}{dt} &= \frac{1}{t} \cdot \frac{da}{dn} \\ \text{and} \quad \frac{da}{dt} &= B \cdot \exp\left(\frac{-Q}{RT}\right) \\ \therefore \frac{da}{dn} &= B \cdot t \cdot \exp\left(\frac{-Q}{RT}\right) \\ \text{so} \quad \ln\left(\frac{da}{dn}\right) &= \ln(t) - \frac{Q}{RT} + \ln(B) \\ \text{let} \quad \alpha(t, T) &= \ln(t) - \frac{Q}{RT} \\ \text{and} \quad B' &= \ln(B) \end{aligned}$$

therefore, the fatigue crack growth rate can be expressed as follows:

$$\ln\left(\frac{da}{dn}\right) = \alpha(t, T) + B' \quad (5)$$

where $\alpha(t, T)$ is termed as the time-dependent factor which is a function of the hold time period of fatigue and absolute temperature under the constant stress intensity factor (K) condition, B' is a

constant if K is kept constant, Q is the thermal activation energy which can be determined in Fig. 9 and 10. In this study, Q was 242 KJ/mole. The time-dependent factor acts as a universal index to associate with fatigue crack growth rates at different temperatures and frequencies.

Based on equation (5), a characteristic curve to describe the FCP under various temperatures and hold time periods can be obtained. Fig. 23 re-plots the measured fatigue crack growth rates of isothermally exposed alloy 783 obtained from Fig. 7 against the time-dependent factor, $\alpha(t,T)$. As exhibited in Fig. 23, all data fall on one curve that consists of two straight lines. The horizontal line with a constant crack growth rate, termed as (da/dn) , represents the cycle-dependent domain. Cyclic stress intensity ΔK is the governed parameter. Paris Law can describe the cycle-dependent FCP behavior as seen in equation (6) ^[9,10]. The other line obtained from sustained load crack growth rate as illustrated in equation (5) displays the time-dependent domain, wherein static stress intensity K_{max} determines the crack growth rate. Equation (5) can describe the time-dependent FCP behavior.

Paris law for cycle-dependent FCP:

$$\frac{da}{dn} = A \cdot \Delta K^n \quad (6)$$

where A is a constant, ΔK is cyclic stress intensity, and n is a material constant.

The empirical expression of time-dependent FCP rate of isothermally exposed alloy 783 can be obtained by linear regression of time-dependent FCP portion in Fig. 23. Results obtained by substitution are shown in Equation (7).

For isothermally exposed alloy 783 at full time-dependent domain:

$$\ln \left(\frac{da}{dn} \right) = \alpha(t, T) + 23.71 \quad (7)$$

The full time-dependent FCP model as shown in Fig.23 provides a simple and straightforward method to characterize the time-dependent FCP behavior. In equation (5), the value of constant,

B' indicates the sensitivity to time-dependent FCP caused by SAGBO. The absolute value of B' is lower, and the resistance to SAGBO induced time-dependent FCP is better. It is interesting to note that fatigue crack propagation behavior of isothermally exposed alloy 783 and as-produced alloy 718 are identical.

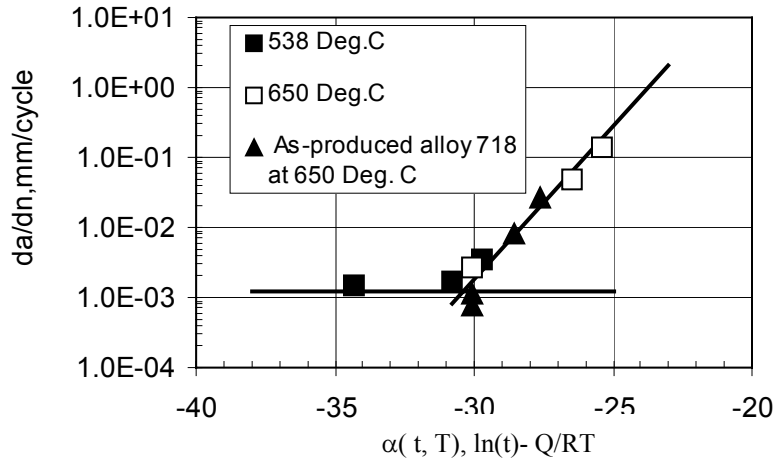


Fig. 23. Normalized FCGR of isothermally exposed alloy 783 and as-produced alloy 718 by time-dependent factor, $\alpha(t, T)$, at $K_{max}=38.5 \text{ MPa}\sqrt{\text{m}}$

Based on equation (5), Fig. 24 compares the FCP rates of as produced and isothermally exposed alloy 783 as a function of time-dependent factor, $\alpha(t, T)$. Since as-produced alloy 783 demonstrates an abnormal time-dependent FCP at 650C° , a single point corresponding to the crack growth retardation appears in Fig. 24. In the time-dependent region, the fatigue crack growth rate can be obtained by linear regression as follows:

For as-produced alloy 783:

$$\ln \left(\frac{da}{dn} \right) = \alpha(t, T) + 23.43$$

The time-dependent FCP behaviors of as-produced and isothermally exposed alloy 783 are unified by the proposed time-dependent factor, $\alpha(t, T)$. When time-dependent factor is small, the crack propagates at the cycle-dependent mode and crack propagates by transgranular fracture

mode. As the time-dependent factor increases, the FCP rate is no longer a constant and increases with the time-dependent factor. In the time-dependent domain, it is of interest to note that offset value of time-dependent factor, wherein the time-dependent FCP starts to occur and fracture path displays intergranular mode. The offset value actually is the value of constant (B') in equation (5). The lower absolute value of B' implies an enhanced resistance to time-dependent FCP. The value of B' is a parameter of material property, and can be controlled through the modification of alloy chemical composition and microstructure. The resistance of materials to the SAGBO induced time-dependent FCP can be determined based on FCP characteristic curves shown in Fig. 24. Prolonged isothermal exposure of alloy 783 marginally decreases resistance to SAGBO induced time-dependent FCP, Fig. 24. However, resistance to SAGBO induced time-dependent FCP of isothermally exposed alloy 783 is identical to as-produced alloy 718.

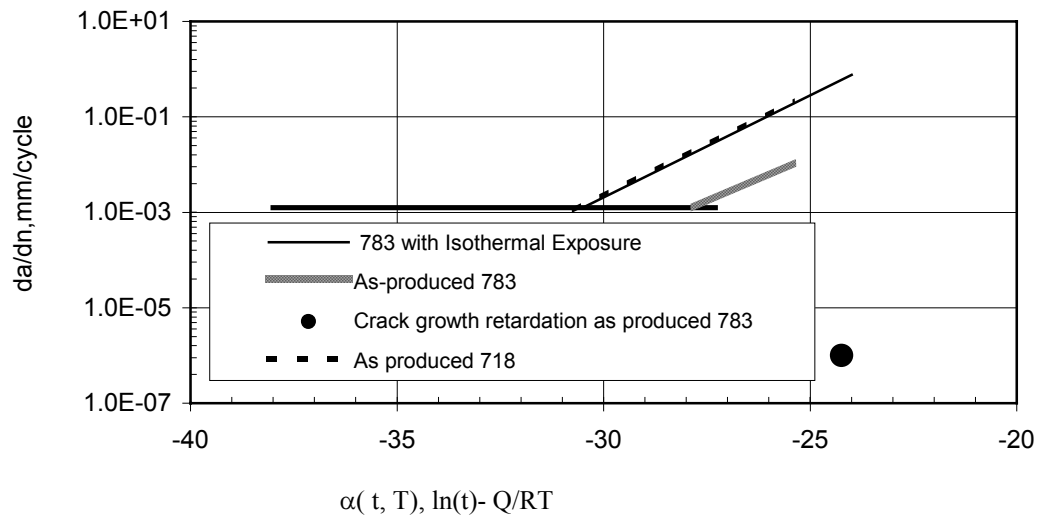


Fig. 24. Characteristic curves to describe FCP behaviors of as-produced and isothermally exposed alloy 783 and as-produced alloy 718.

V. Conclusions

The time-dependent FCP behaviors of isothermally exposed and as produced INCONEL alloy 783 were investigated comprehensively at elevated temperature. A full time-dependent FCP model was proposed to characterize the FCP behavior. The experimental work and analysis results suggest the following conclusions:

1. Both isothermally exposed and as-produced alloy 783 display the time-dependent FCP behaviors at elevated temperature when a hold time fatigue load is introduced.
2. Under prolonged hold time and sustained loading conditions, as-produced alloy 783 exhibits a crack growth retardation phenomenon but isothermally exposed alloy 783 demonstrates a steady sustained loading crack growth typically observed in as-produced superalloys such as alloys 718 and 706.
3. Resistance to SAGBO induced time-dependent FCP of isothermally exposed alloy 783 was identical to as-produced alloy 718.
4. The existence of a damage zone ahead of crack tip caused by sustained loading was confirmed. The formation of damage zone, sustained loading crack growth and incubation processes are related with the rate-controlled thermal activation process. The formation and propagation of a damage zone governs the time-dependent FCP process.
5. A full time-dependent FCP model, by introduction of the time-dependent factor, $\alpha(t, T) = \ln(t) - Q/RT$, can normalize the hold time (t) and temperature (T) to unify the FCP data for all alloys. Two characteristic curves describing the FCP processes of as-produced and isothermally exposed alloy 783 determine the resistance to time-dependent FCP.

Acknowledgements

This work was supported by Air Force Office of Scientific Research, Arlington, VA 22203 under Grant No. F49620-99-1-0274 and the West Virginia EPSCOR program. Special Metals

Corporation, Huntington, WV is thanked for in-depth review of this manuscript and technical coordination throughout this work.

References

1. J. S. Smith and K. A. Heck: Superalloys 1996, R. D. Kissinger, D. J. Deye, D. L. Anton, A. D. Cetel, M. V. Nathal, T. M. Pollock, and D. A. Woodford ed., TMS, Seven Spring, PA, USA, 1996, pp. 91-100.
2. K. A. Heck, J. S. Smith, R. L. Smith: International Gas Turbine and Aeroengine Congress & Exhibition, Birmingham, UK, June 10-13, 1996, pp. 1-8.
3. K. A. Heck, D. F. Smith, M. A. Holderby and J.S. Smith: Superalloy 1992, S. D. Antolovich, R. W. Stusrud, R. A. Mackay, D. L. Anton, T. Khan, R. D. Kissinger, D. L. Klarstrom, ed., TMS, Seven Springs, PA, USA, 1992, pp. 217-226.
4. S. Mannan and J. deBarbadillo: International Gas Turbine and Aeroengine Congress & Exhibition, Stockholm, Sweden, June 2-5, 1998, pp. 1-10.
5. J. F. Radavich and Andrea Fort: Superalloy 718, 625 and Various Derivatives, E. A. Loria, ed., TMS, Warrendale, PA, USA, 1994, pp. 635-647.
6. D. Zheng and H. Ghonem: Metall. Trans., Vol. 23 A, Nov. 1992, pp. 3169-3171.
7. H. H. Smith and D. J. Michel: Metall. Trans., Vol.17A, Feb. 1986, pp. 370-374.
8. H. Ghonem and D. Zheng: Mater. Sci. and Eng. A150, 1992, pp. 151-160
9. K.-M. Chang, M. F. Henry and M. G. Benz: JOM, Dec.1990, pp. 29- 35.
10. K.-M. Chang: G.E R & D Report, No: 91CRD066, March 1991, pp. 1-19.
11. J. F. Barker, E. W. Ross, and J. F. Radavich: J. Metals, Jan. 1970, pp. 31-34.
12. K. Sadananda and P. Shahinian: Metall. Trans., Vol 8A, March 1977, pp. 439-449.
13. Jed S. Lyons, Anthony P. Reynolds and James D. Clawson: Scripta Materialia, Vol. 37, No. 7, 1997, pp. 1059-1064.
14. T. Nicholas and T. Weerasooriya: in Fracture Mechanics, Vol. 17, ASTM STP 905, 1986, pp. 155-168.

15. Shyuan-Fang Chen and Robert P. Wei: *Mater. Sci. Eng. A256* (1998), pp. 197-207.
16. P. Valerio, M. Gao and R. Wei: *Scripta Metall. et Mater.*, Vol. 30, 1994, pp.1269-1274.
17. S. Floreen and R. H. Kane: *Metall. Trans.*, Vol 13A, Jan. 1977, pp.145-152.
18. George E. Dieter: *Mechanical Metallurgy*, McGraw Hill Press, 1986, pp. 309-310.
19. L. Z. Ma, K.-M. Chang, S.K. Mannan: *Advanced Technologies for Superalloy Affordability*, K.-M. Chang, S.K. Srivastava, D.U.Furrer and K.R. Bain, ed., TMS Annual Meeting, Nashville, TN, March 2000, pp. 131-140.
20. L. Z. Ma, K.-M. Chang, S. K. Mannan, S. J. Patel: *Superalloy 2000*, T.M. Pollock, R.D. Kissinger, P.R. Bowman, K.A. Green, M. McLean, S. Olson and J. J. Schira, ed., TMS, Seven Springs, PA, Sept. 2000, pp. 601-609.
21. Xingbo Liu, Longzhou Ma and Keh-Minn Chang: *Superalloys 718, 625, 706 and Various Derivatives*, E.A. Loria, ed., TMS, Warrendale, PA, 2001, pp. 543-552.
22. E.W.A. Young and J. H. W. de Wit: *International Congress on Metallic Corrosion*, 9th, Toronto, Canada, 1984, pp. 50-53.
23. P.A. van Manen, E. W. A. Young, D. Schalkoord, C. J. van der Wekken and J. H. W. de Wit: *Surface and Interface Analysis*, Vol. 12, 1988, pp.391-396.
24. E. W. A. Young, J. C. Riviere and L. S. Welch: *Applied Surface Science* 31, 1988, pp. 370-374
25. Bruce A. Pint, Anthony J. Garratt-Reed, and Linn W, Hobbs: *J. Am. Ceramic. Soc.* 81[2], 1998, pp. 305-314.
26. P. E. Irving, J. L. Robinson, and C. J. Bevers: *Eng. Fract. Mech.* Vol. 7, 1975, pp. 619-630.
27. T. T. Shih and R. P. Wei: *Eng. Fract. Mech.* Vol. 6, 1974, pp. 19-32.
28. S. Suresh: *Fatigue of Materials*. Cambridge University Press, 1991.
29. H. J. Grabke: *Intermetallics* 7, 1999, pp. 1153-1158.

List of Figures and Tables

Table I: Chemical Composition of INCONEL alloy Alloy 783 (wt%)

Table II: Comparison of Tensile Properties and Hardness at Room Temperature

Fig. 1: Schematic illustration of FCP test procedure

Fig. 2: Schematic illustration of damage access test

Fig. 3: Optical microstructure of alloy 783; (a). Isothermally exposed ; (b). As-produced

Fig. 4: SEM micrograph of β precipitate in alloy 783; (a). Isothermally exposed; (b). As-produced

Fig. 5: FCP curves of isothermally exposed alloy 783 at $K_{max}=38.5 \text{ MPa}\sqrt{\text{m}}$ and 650°C

Fig. 6: Fatigue crack growth rate of alloy 783 as a function of period, S; (a) Isothermally exposed; (b) As-produced

Fig. 7: Comparison of fatigue crack growth rate between isothermally exposed and as-produced alloy 783 at $K_{max}=38.5 \text{ MPa}\sqrt{\text{m}}$

Fig.8: Damage access result of isothermally exposed alloy 783 at $K_{max}=38.5 \text{ MPa}\sqrt{\text{m}}$; (a).

Sustained loading crack growth at 650°C ; (b). Damage zone identification at room temperature

Fig. 9: da/dt of isothermally exposed alloy 783 vs. $1/T$ and $1/t_i$ vs. $1/T$

Fig.10: da/dt of isothermally exposed alloy 783 vs. $1/T$ and damage zone size vs. $1/T$

Fig.11: Damage access result of as produced alloy 783 at $K_{max}=38.5 \text{ MPa}\sqrt{\text{m}}$; (a) Sustained loading crack growth retardation at 650°C ; (b) Delayed FCP following (a) at room temperature

Fig.12: FCP curves of as- produced alloy 783 at $K_{max}=38.5 \text{ MPa}\sqrt{\text{m}}$, $R=0.05$ and 650°C

Fig.13: Time-dependent FCP of alloy 783 at $K_{max}=38.5 \text{ MPa}\sqrt{\text{m}}$ and 650°C

Fig.14: Time-dependent FCP of alloy 783 at $K_{max}=38.5 \text{ MPa}\sqrt{\text{m}}$ and 538°C

Fig. 15: Tensile stress relaxation of alloy 783 at 650°C

Fig. 16: SEM fracture surface micrograph of isothermally exposed alloy 783 at 650°C ; (a): 3s ; (b): 3+100s ; (c): 3+300s ; (d): Sustained loading

Fig. 17: SEM fracture surface micrograph of as-produced alloy 783; (a): At 3+100s and 650°C; (b): At 650°C; (c) High magnification of (b); (d): At 3+300s and 538 °C

Fig. 18: SEM micrograph of as-produced alloy 783 at 650 °C; (a). Crack extension region at 3+1000s; (b). High magnification of (a) at 3+1000s

Fig. 19: Sustained loading crack growth retardation of as produced alloy 783 at 650 °C; (a). Optical micrograph of crack path; (b).SEM fracture surface micrograph of (a)

Fig. 20: TEM micrograph of β precipitate in alloy 783; (a) As produced; (b) isothermally exposed

Fig. 21: Voltage change during fatigue crack growth test at $K_{max}=38.5\text{MPa}\sqrt{\text{m}}$, $R=0.05$ and 650°C; (a): Voltage and load change within a fatigue cycle with a period of 3s; (b): Potential drop at minimum load, Ψ , as a function of cycle number

Fig. 22: Schematic illustration of the sustained loading crack growth governed by damage zone; (a). Formation of a critical damage zone during incubation; (b). Crack growth by consecutive formation and propagation of a damage zone

Fig. 23: Fatigue crack growth rate normalized of isothermally exposed alloy 783 by time-dependent factor, $\alpha(t, T)$, at $K_{max}=38.5\text{MPa}\sqrt{\text{m}}$

Fig. 24: The characteristic curves to describe FCP behaviors of alloy 783